Methane condensation influences the thermal histories of Uranus and Neptune

Steve Markham and Dave Stevenson

September 23, 2020

Abstract

The internal heat flows of both Uranus and Neptune remain major outstanding problems in planetary science. Uranus' surprisingly cold effective temperature is inconsistent with adiabatic thermal evolution models, while Neptune's substantial internal heat flow is twice its received insolation. In this work we demonstrate that convective inhibition by methane condensation partially decouples these planets' photospheres from their interiors. In the case of methane, this decoupling allows the atmosphere to rapidly cool while the interior remains hot. This effect can reduce the thermal age of Uranus or Neptune inferred by their luminosities by nearly a factor of two. If water condensation inhibits convection by a similar mechanism deeper in the atmosphere, the effect is in the opposite direction. In the case of water, convective decoupling causes the interior to lose heat less efficiently, slowing the thermal evolution process and increasing the thermal age of Uranus or Neptune by more than 50%. Additional deep condensing layers, for example silicates, will likewise slow thermal evolution like water if they are sufficiently abundant to inhibit convection. These general principles should apply to the thermal histories of any planet with a hydrogen atmosphere sufficiently polluted with volatile species, such as super-Earth and Neptune-like exoplanets. If convective inhibition by condensation indeed occurs in Uranus and Neptune's envelopes, then it is an essential consideration to understand their thermal histories, internal structure, and contemporary heat flows.

1 Introduction

Giant planet atmospheres are primarily heated by a combination sunlight and internal heat leftover from formation. All giant planets except Uranus are observed to emit more infrared radiation into space than the absorbed sunlight, by approximately a factor of two. Jupiter's present day luminosity can be approximately explained by convective cooling from an initially hot state over the age of the solar system [Hubbard, 1977][Hubbard et al., 1999]. To accurately reproduce Saturn's present day state, one may need to account for additional heating by the settling of helium rain from the envelope into the interior

[Hubbard et al., 1999][Stevenson, 1983]. However, luminosity is a crude indicator of thermal evolution since planets can store heat internally and may have internal heat sources (e.g. differentiation). The present luminosities of Uranus and Neptune are not well understood because even their basic structures are not well understood.

Measurements of the ice giants' electromagnetic emission to space began in the 1960s [Kellermann and Pauliny-Toth, 1966], with high quality far infrared measurements constraining the effective temperatures beginning in the 1970s [Fazio et al., 1976][Loewenstein et al., 1977][Stier et al., 1978]. These early observations concluded that Uranus appeared approximately in equilibrium with its received sunlight, while Neptune emitted more than twice the radiation it received. These observations were corroborated by higher quality analysis after the Voyager 2 flybys [Pearl et al., 1990][Pearl and Conrath, 1991]. The 1σ upper limit for Uranus' energy balance (the ratio between its emitted and absorbed thermal flux) is 1.14. The lower limit is below unity, indicating the results are consistent with zero internal heat flow. However, we know the heat flow cannot be zero because Uranus has a magnetic field. Moreover, the higher microwave temperatures at long wavelengths (e.g. [Gulkis et al., 1983]) are compatible with heat flow from depth. Uranus *must* be convective at depth.

Theoretical attempts to explain these observations began promptly. It was immediately clear that the ice giants could not have the same thermal histories as the gas giants. Early studies concluded that, if these planets cool convectively like the gas giants, they must have formed at a temperature not much warmer than their current states [Hubbard, 1978][Hubbard and MacFarlane, 1980], a highly unlikely interpretation because the energy of accretion $\sim GM^2/R$ far exceeds their current heat content for any plausible assumption of structure. Alternative theories suggested a large fraction of gravitational heat of formation remains trapped in the interior, but by some mechanism cannot escape to space [Podolak et al., 1991]. More recent studies suggest that there is no problem for Neptune [Fortney et al., 2011][Linder et al., 2019], or even that Neptune's present luminosity is higher than expected [Nettelmann et al., 2016][Scheibe et al., 2019]. Uranus' very low internal heat flux, sometimes known as the faintness problem [Helled et al., 2020], remains largely unsolved, although it has been suggested that the problem can be solved by modeling thin layers of static stability near phase boundaries [Nettelmann et al., 2016]. Today it is largely accepted that the adiabatic assumption for the interior is probably inappropriate for Uranus and Neptune [Helled et al., 2020].

In this work we present a mechanism that inhibits convection near the methane cloud level, thereby trapping internal heat beneath the clouds. This mechanism has already been theorized and discussed e.g. [Leconte et al., 2017] [Friedson and Gonzales, 2017] [Guillot, 2005], but the effect of methane on the ice giants has not yet been explicitly quantified and worked into a thermal evolutionary model. In hydrogen atmospheres, sufficiently abundant condensible

species can shut off convection near the cloud level [Guillot, 1995][Guillot, 2005]. By "sufficiently abundant" we mean greater than an analytically calculable critical mole fraction $q_{\rm crit}$. This value is about 1.4% for methane and 1.2% for water under the relevant conditions in Uranus and Neptune. Recent theoretical study confirms this effect is stable to double diffusive convection [Leconte et al., 2017][Friedson and Gonzales, 2017]. Methane is certainly sufficiently abundant for convective inhibition to occur [Helled et al., 2020]. The long-term survival of the configuration against entrainment is still a subject of research; the configuration may be intermittently eroded, destroyed, and reformed [Friedson and Gonzales, 2017].

In Section 2, we quantify the effect of convective inhibition by methane as a function of methane abundance and planetary internal temperature. In Section 3, we use this information to provide a correction to standard adiabatic thermal evolution models. In Section 4 we present the results for methane, demonstrating that this effect can indeed reduce the cool down time from an initially hot state to the present state of the ice giants by nearly 50%. In Section 5 we assess the possible role of water condensation in thermal evolution, finding its effect to counter-intuitively be opposite to methane's. That is, accounting for water condensation actually lengthens the cooling time from an initially hot state to the present luminosities of the planets. We then present evolution results when considering both water and methane condensation simultaneously. Finally in Section 6 we discuss the implications of these results for thermal evolutionary models of the ice giants, and discuss the application of this work in the broader context of thermal evolution models.

2 Atmospheric model

We model a radiative-convective equilibrium atmosphere using a two stream gray opacity approximation for thermal radiative transfer. We seek to uniquely define the apparent effective temperature T_e as a function of a planet's internal equivalent effective temperature $T_{\rm int}$ and condensate abundance $q_{\rm max}$. By $T_{\rm int}$ we mean the effective temperature the planet would have if convective inhibition by condensation did not occur. T_e is the actual effective temperature one would observe for an atmosphere in radiative-convective equilibrium that accounts for convective inhibition by condensation. Planetary and physical properties, such as surface gravity and the physical properties of the gas mixture, are considered to be fixed.

We also assume the planet is subject to intermittent moist convective events that overcome the potential barrier of the stable layer. These could occur due to instabilities caused by entrainment over long timescales [Friedson and Gonzales, 2017], rare impact events, or strong updrafts from the interior. The equilibrium configuration then is reached by gradual cooling, with the upper layer relaxing onto a moist pseudo-adiabat set by a different potential temperature than the adiabat that sets the interior. The stable layer meanwhile will have a super-adiabatic

temperature gradient set by thermal radiative equilibrium, see Figure 2.

2.1 Defining the boundaries of the stable layer

This work investigates the effect of convective inhibition on thermal evolution. In this subsection we quantify important pressure boundaries we need to define the radiative transfer model in the following subsection. The key idea here is that the condensate mixing ratio $q_{\rm crit}$ needed to provide a region of static stability is less than the mixing ratio in a much deeper well mixed region $q_{\rm max}$. We consider an atmosphere where optical depth unity in the IR is at lower pressure than the level at which convection is expected. At deeper levels (higher pressure) we assume there is a region of rapidly varying condensate mixing ratio in the vapor phase; this region can be convectively stable as we show below. Deeper still, below the conventionally defined cloud deck, the condensate mixing ratio the condensate mixing ratio is a constant because the vapor pressure is always less than the saturated vapor pressure at that temperature. We refer to this below as the "bulk mixing ratio" though it is strictly only applicable to whatever deep, well mixed layer lies beneath the clouds and says nothing about the actual methane abundance at far deeper levels (i.e., the methane abundance of the planet as a whole). Accordingly, our atmosphere has (from the top downward) a radiative zone (the stratosphere) a convective zone, another radiative zone (called the 'stable layer' below) and a deep convective zone. The sunlight in the methane model is assumed to be absorbed completely below the cloud deck. This is justified because the atmosphere is less opaque in the visible spectrum compared to the infrared spectrum by more than two orders of magnitude. In reality some sunlight is absorbed in the shallow layer; for this reason, these results should be thought of as an upper bound of the magnitude of this effect, as sunlight absorbed above the stable layer will reduce the required temperature difference across the stable layer by reducing the total heat flux that must be accommodated.

Under the Eddington approximation, the thermal structure of an atmosphere in radiative equilibrium as a function of optical depth is $T(\tau) = T_e(3\tau/4 + 1/2)^{1/4}$. We assume the IR opacity to be dominated by pressure-induced opacity of hydrogen collisions that approximately obeys $\kappa \sim \kappa_0(p/p_0)$, where $\kappa_0 = 10^{-2}\mathrm{g}^{-1}\mathrm{cm}^2$ and $p_0 = 1$ bar. An atmosphere in radiative equilibrium becomes unstable to convection at the point where its lapse rate becomes superadiabatic. For a dry adiabatic atmosphere, the potential temperature $\theta(p,T) = T(p_0/p)^{R/c_p}$ is constant at all levels, where R is the specific gas constant of the gas mixture and c_p its constant pressure specific heat capacity. Under our assumptions, this places the pressure level of the radiative-convective boundary

$$p_{\rm rc}^2 = \frac{8gp_0R}{3(c_p - 2R)\kappa_0} \tag{1}$$

We use a dry adiabatic lapse rate to set the radiative-convective boundary be-

cause we assume the effect of moist adiabaticity is small in this relatively cold part of the atmosphere. Beneath the boundary, we assume the atmosphere to be moist adiabatic. A moist adiabatic atmosphere conserves the equivalent potential temperature

$$\theta_e(p,T) = \theta(p,T)\exp\left[\frac{\epsilon e(T)}{c_p T(p-e(T))}\right] \tag{2}$$

where ϵ is the mass ratio of the condensate to the dry gas mixture, and $e(T) = p_0 \exp\left[\frac{L}{R}\left(\frac{1}{T_b}-\frac{1}{T}\right)\right]$ is the Clausius-Clapeyron saturation vapor pressure. L is the latent heat, p_0 is 1 bar and T_b the 1 bar boiling temperature of the condensate. We set the moist adiabatic equivalent potential temperature using the temperature and pressure at the radiative-convective boundary. By doing this, we define a unique moist adiabat for a given effective temperatures. The difference between the two adiabats is the difference between the internal equivalent effective temperature $T_{\rm int}$ and the apparent effective temperature T_e.

A hydrogen atmosphere becomes unstable to convection at a temperature dependent critical value of the condensate mole fraction $q_{\rm crit}$ that depends on the properties of the condensate and the gas mixture [Guillot, 1995] [Friedson and Gonzales, 2017] [Leconte et al., 2017]. The mechanism is as follows: consider an isobaric open system hydrogen gas parcel saturated with a vapor species of higher molecular weight. Assume there exists a finite reservoir of liquid condensate in equilibrium with the saturated parcel, outside but in contact with the system. If the parcel is relatively cool, the effect of the condensate will be a small correction, and the parcel will approximately behave like an ideal gas such that density decreases as temperature increases. However, as temperature increases at fixed pressure, the mixing ratio of the condensate likewise increases. Because the condensate vapor is heavier than the dry air, there comes a crossover where the Arrhenius relationship in temperature governing vapor pressure saturation overcomes the linear relationship in temperature governing mean spacing between molecules in a gas. After this crossover point for the system outlined above, increasing temperature actually increases the density of the parcel. For this reason, a hydrogen atmosphere with sufficiently abundant condensate ($q_{\rm max} > q_{\rm crit}$) with an internal heat source will not convect. It does not convect because the warmer underlying gas is Ledoux stable to convection for any temperature gradient if saturated at all levels.

Since we have an ideal gas, the mole fraction of the condensate must satisfy $q(p,T) = e(T)/p(T)$ in equilibrium. Note that the mole fraction, which we call q, is not the same as the variable defined as q in [Leconte et al., 2017]. When we define a moist adiabat, the temperature is uniquely defined at every pressure level. Therefore we can solve for the level p_1 where the atmosphere becomes stable to convection by solving $q(p_1) = q_{\rm crit}(T(p_1))$. In our notation,

$$q_{\rm crit}^{-1} = \left(\frac{\epsilon L}{RT} - 1\right)(\epsilon - 1) \tag{3}$$

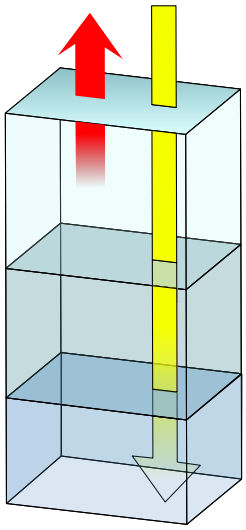

Figure 1: A cartoon basic representation of the model. Thermal radiation to space comes from the upper layer, while sunlight is absorbed by the deep layer. These layers are convectively decoupled by the stable cloud layer.

Similarly, we can solve for the bottom of the stable layer by solving $q(p_2) = q_{\rm max}$, where $q_{\rm max}$ is the bulk abundance of the condensate species. This is set using the pseudoadiabat corresponding to a planet with effective temperature $T_{\rm int}$ neglecting convective inhibition. This is the sense in which we mean "internal equivalent effective temperature", because it neglects the effect of convective inhibition but is still set using an equivalent effective temperature. We will demonstrate in general for cases in which $q_{\rm max} > q_{\rm crit}$, and where the condensate condenses in the convective part of the atmosphere, in equilibrium p_1 and p_2 will be set using different effective temperatures. They are set using T_e and $T_{\rm int}$, respectively.

Figure 2 contains apparent temperature discontinuities, which exist in the model. Of course, temperature discontinuities are not stable in natural media, as conductive heat transport will be infinite. Additionally, a temperature discontinuity–even if stabilized by a compositonal difference–will lead to negligible temperature differences due to thin thermal boundary layer convection in an inviscid fluid. The temperature discontinuities in Figure 2 therefore do not actually represent discontinuities in nature, but steep temperature gradients. We provide the following order of magnitude analysis to determine how important these steep quasi-discontinuities are in the context of the model. The relaxation timescale for thermal diffusion in a medium with thermal conductivity k_t is

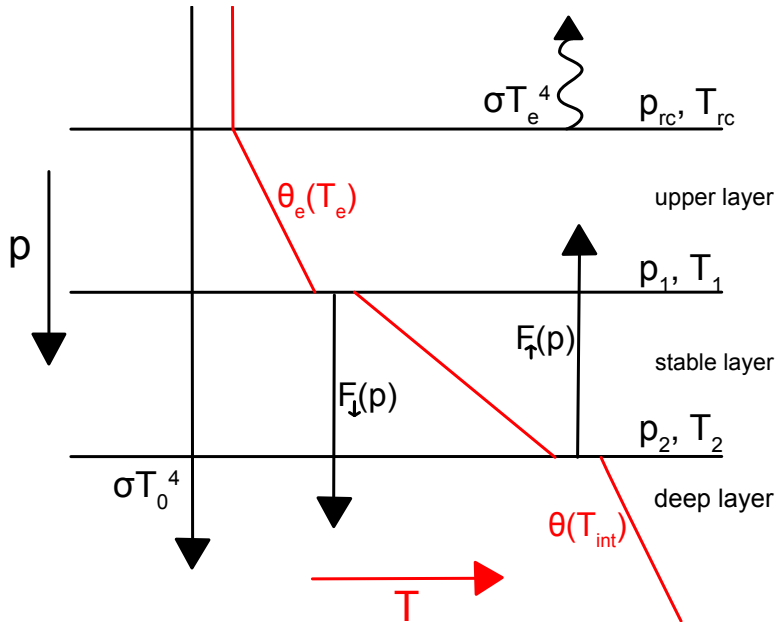

Figure 2: A schematic sketch of the model (not to scale). The red curves represent temperature increasing to the right, with the moist pseudo-adiabatic temperature set using an equivalent potential temperature derived from the planets' apparent effective temperature T_e. The deep layer temperature structure is set using the potential temperature derived from the internal equivalent potential temperature $T_{\rm int}$. The superadiabatic temperature gradient in the stable layer is set by solving for local radiative thermal equilibrium. The horizontal black curves correspond to important pressure levels, with pressure increasing downward. The interface between the upper moist convective layer and stable layer is p_1, with a local temperature T_1. The interface between the deep dry convective layer is p_2, with a local temperature of T_2. The system is in equilibrium when $F_\uparrow(p_1) - F_\downarrow(p_1) = \sigma(T_e^4 - fT_0^4)$, where f is the fraction of sunlight absorbed above the stable layer and T_0 is the equilibrium effective temperature with sunlight in the absence of internal heat.

$\tau_c \sim \frac{\rho c_p L^2}{k_t}$, where L is the vertical length scale of relevance. The timescale for radiative relaxation is the radiative time constant $\tau_{\rm rad} \sim \frac{c_p}{8\sigma T^3 \kappa}$. We solve for the thickness of the conductive layer by equating the two timescales solving for L. Using appropriate parameters for hydrogen around 1 bar ($k_t \sim 10^4$g cm s^{-3} K^{-1}, $\rho\kappa \sim 10^{-6}$) we find the length scale to be of order 10-100 meters, small compared to atmospheric length scales (i.e., the scale height). Then using Fourier's Law, we find heat conduction to be of order 10^{-2}erg cm^{-2} s^{-1} for discontinuities of order 1K (scaling linearly with the size of the temperature discontinuity), about four orders of magnitude smaller than σT_e^4 and therefore not included in the model. Thus the discontinuities in Figure 2 are really there in the model, but are physically understood to be steep temperature gradients nevertheless unimportant for the purposes of calculating total heat flow.

We must also comment on entrainment by convection outside the stable layer. Entrainment will tend to erode and thin the stable layer over time [Friedson and Gonzales, 2017]. In general for water, the erosion timescale is greater than the cooling timescale, indicating that the equilibrium configuration should exist at some times. However as the stable layer is eroded and becomes thinner, heat transport across the stable layer will be enhanced, reducing the difference between T_e and $T_{\rm int}$. Eventually the thinning stable region will reduce to an interface that may be stable, unstable, or conditionally stable. We acknowledge that these complications are confounding factors for our model, and therefore our results that neglect entrainment erosion of the stable layer should be thought of as an upper bound on the magnitude of the effect on ΔT and on evolution.

The equilibrium solution will be stable if the virtual potential temperature θ_v is monotonically decreasing with increasing pressure between p_1 and p_2.

$$\theta_v(p,T) = T_v(p,T)\left(\frac{p_0}{p}\right)^{R/c_p} \tag{4}$$

$$T_v(p,T) = T\left(1 - q(1-\epsilon)\right)^{-1} \tag{5}$$

In the equilibrium cases discussed here, this condition is always satisfied. It is worth noting that this is not necessarily true in general; if $q_{\rm max} \sim q_{\rm crit}$ the behavior can become that of a relaxation oscillator, with period of stability interrupted by short periods of violent convective activity that rapidly releases a large amount of potential energy (e.g. [Li and Ingersoll, 2015]). In our case, we consider cases where $q_{\rm max}$ is sufficiently greater than $q_{\rm crit}$, so that this relaxation behavior is not exhibited, and a radiative-convective equilibrium state can be attained that retains a permanent stable layer.

2.2 Radiative transfer across the stable layer

Figure 2 is a useful visual reference for this section. In order to compute the radiative-convective equilibrium solution, we first solve for the equilibrium heat

flow for a system specifying the boundaries of the stable layer p_1 and p_2, along with their corresponding temperatures T_1 and T_2. The temperature structure above p_1 is moist adiabatic, while the temperature structure below p_2 is dry adiabatic. In equilibrium $\frac{dT}{dt} \propto \frac{dF}{dp} = 0$. Then using the two stream approximation of radiative transfer

$$\frac{dF}{dp_\uparrow} = \frac{dF}{dp_\downarrow} = \frac{\kappa}{2g}(F_\uparrow - F_\downarrow) \tag{6}$$

With appropriate boundary conditions, we can analytically solve for the upward and downward heat flux at every level in the stable layer. Of interest for our problem is the net heat flow from the deep/stable layers to the shallow layer that is convectively coupled to the photosphere. This is

$$F_\uparrow(p_1) - F_\downarrow(p_1) = \frac{4F_2 g p_0 + F_1(p_2^2 - p_1^2)\kappa_0}{4gp_0 + (p_2^2 - p_1^2)\kappa_0} - F_1 \tag{7}$$

where $F_1 = F_\downarrow(p_1)$ and $F_2 = F_\uparrow(p_2)$ are the boundary conditions. We can solve for these boundary conditions using the uniquely determined temperature structures above and below the stable layer, i.e.

$$F_1 = \frac{\kappa_0 \sigma}{g} \int_0^{p_1} \exp\left[\frac{\kappa_0(p^2 - p_1^2)}{2gp_0}\right] T(p)^4 (p/p_0) dp \tag{8}$$

$$F_2 = \frac{\kappa_0 \sigma T_2^4}{g} \int_{p_2}^{\infty} \exp\left[\frac{\kappa_0(p_2^2 - p^2)}{2gp_0}\right] (p/p_2)^{4R/c_p} (p/p_0) dp \tag{9}$$

Using this process, for a given $(T_{\rm int}, q_{\rm max}) \implies (p_2, T_2)$ we solve the above nonlinear equation to obtain $T_e \implies (p_1, T_1)$ using the condition $F_\uparrow(p_1) - F_\downarrow(p_1) = \sigma(T_e^4 - fT_0^4)$ where f is the fraction of sunlight absorbed above the stable layer, and T_0 is the equilibrium effective temperature with the sun in the absence of internal heat. This defines the apparent effective temperature as a function of the internal equivalent effective temperature $T_e(T_{\rm int})$ shown in Figure 3 using $\Delta T \equiv T_e - T_{\rm int}$.

Finally we must consider the deposition of sunlight. The primary absorber of sunlight in Uranus' troposphere is methane vapor [Marley and McKay, 1999], while the primary absorber of infrared light is hydrogen collisions. At 1 bar with 2% methane for example, accounting for methane absorption plus Rayleigh scattering vs. thermal absorption by hydrogen, the ratio between visible to thermal infrared opacity is approximately $\kappa_\odot/\kappa_t < 10^{-2}$ averaging over a broad band in wavelength. This value of course is not unique; there are windows at certain wavelengths, the methane abundance changes rapidly with depth, and this simple calculation neglects absorption by haze and cloud particles. Nevertheless $\kappa_\odot/\kappa_t$ is sufficiently small that we can plausibly argue that sunlight penetrates significantly beyond the 1 bar level, and most of the sunlight is absorbed deeper in the atmosphere. This can be parameterized by simply arguing some fraction f of sunlight is absorbed above the cloud level, and $1 - f$ is absorbed below. In principle this procedure accommodates any value of f, but for our purposes

for simplicity we approximate using the limiting cases $f \to 0$ for the shallow ($\sim$ 1bar) methane condensation level, while $f \to 1$ for deep ($\sim$ 100bar) water clouds. The difference for the stable layer is that in radiative equilibrium, the flux through the stable layer must balance with $\sigma(T_e^4 - fT_0^4)$ as explained above. When we consider methane and water clouds simultaneously, we assume the sunlight is primarily absorbed below the methane condensation level but above the water clouds in Section 5.

3 Evolutionary model

We present an adiabatic thermal evolution model of Uranus and Neptune. As discussed, treating the interior as adiabatic is probably inappropriate for the ice giants [Helled et al., 2020]. Nevertheless it provides a convenient framework to understand the effect of methane condensation on these planets' thermal histories in the absence of an accepted interior model. For an adiabatic model, we assume the total heat content of the planet's interior to be a linear function of its internal equivalent effective temperature $T_{\rm int}$.

$$\int_{M_{\rm min}}^{M} c_p T dm = A\bar{c_p} M T_{\rm int} \tag{10}$$

One way of thinking about this equation is to imagine a small set of layers, or possibly even one layer, in the form of concentric shells, each of which is isentropic and homogeneous but of different composition to neighboring layers, with negligible thermal boundary layers between them as would be fluid dynamically expected for a low viscosity system. Beneath this set of shells there could be a region, possibly a substantial fraction of the planet, where there is a compositional gradient and therefore inefficient convective transport. This deeper region would not contribute to A or to the resulting thermal evolution of the planet because it stores primordial heat. The parameter A then is approximately constant through time because the Gruneisen parameter is rather insensitive to temperature, and its value is set by the fraction of the total mass that is fully convective. This approach is not guaranteed to correctly describe the behavior of an ice giant since we do not know the internal structure. It is likely to be thermodynamically impossible [Bailey and Stevenson, 2020]. However, it serves our purpose because it enables us to focus on a specific effect: the changing relationship of $T_{\rm int}$ relative to T_e as clouds form.

The rate of cooling depends on the apparent effective temperature T_e. The equation governing thermal evolution is then

$$4\pi R^2 \sigma (T_e^4 - T_0^4) = -A\bar{c_p} M \frac{dT_{\rm int}}{dt} \tag{11}$$

where T_0 is the equilibrium effective temperature of the planet with sunlight if there were no internal heat source. The radius R is treated as constant because

we are concerned with most of the evolution where the body is degenerate, not any early very hot phase. The steady increase in solar luminosity (i.e. time variation of T_0) is ignored. In order to solve the thermal evolution equation, we need an explicit relationship between T_e and $T_{\rm int}$. This is done using the method from Section 2, with the results for methane in Figure 3 and for water in Section 5. We also present the combination of both effects simultaneously in Section 5. In general the relationship between T_e and $T_{\rm int}$ depends on the condensate bulk interior abundance $q_{\rm max}$. Without condensation, the relationship is $T_e = T_{\rm int}$. In this case, Equation 11 can be non-dimensionalized into the canonical form

$$\frac{x^4 - x_0^4}{1 - x_0^4} = -\tau_K \frac{dx}{dt} \tag{12}$$

where $x \equiv T_e/T_e^{(\emptyset)}$ where $T_e^{(\emptyset)}$ is the apparent effective temperature today, and $x_0 = T_0/T_e^{(\emptyset)}$. The Kelvin timescale $\tau_K = \frac{A\bar{c_p}MT_e^{(\emptyset)}}{4\pi R^2 \sigma}(T_e^{(\emptyset)4} - T_0^4)^{-1}$ scales how long it takes to cool to $T_e^{(\emptyset)}$ from an initial arbitrarily hot state. In the asymptotic case $T_e^{(\emptyset)} \gg T_0$ (not true for Uranus!), this is about $\tau_K/4$, but can be a different fraction of τ_K in general.

Accounting for condensation, Equation 11 becomes

$$\frac{dx}{dx_{\rm int}} \frac{x^4 - x_0^4}{1 - x_0^4} = -\tau_K \frac{dx}{dt} \tag{13}$$

where $x_{\rm int} = T_{\rm int}/T_e^{(\emptyset)}$. The difference between Equations 12 and 13 then straightforwardly demonstrates the effect of convective inhibition by condensation on the planets' thermal evolution: it alters the rate of cooling by a factor of $\frac{dx}{dx_{\rm int}}$. As we will see, this factor can be greater than or less than unity. This means the effect can either speed up or slow down the rate of change of the planets' apparent effective temperature at different points in the its thermal history. This is especially important for understanding the results from Section 5.

The fact that Equation 13 retains the Kelvin timescale τ_K makes this formulation especially convenient. This allows us to directly compare the fraction of that timescale that a given evolutionary model takes to cool from arbitrarily hot bodies to their current temperatures for different assumptions of the condensate abundance $q_{\rm max}$. Leaving the the effect in terms of the Kelvin timescale allows our results to be roughly independent of accurate interior models.

4 The effect of methane condensation

Provided $q_{\rm max} > q_{\rm crit}$, when the planet cools to an internal equivalent effective temperature $T_{\rm int}$ of 65K to 75K, depending on bulk methane abundance in the envelope, convection is interrupted. At this point the apparent effective temperature departs from the internal equivalent effective temperature, by the

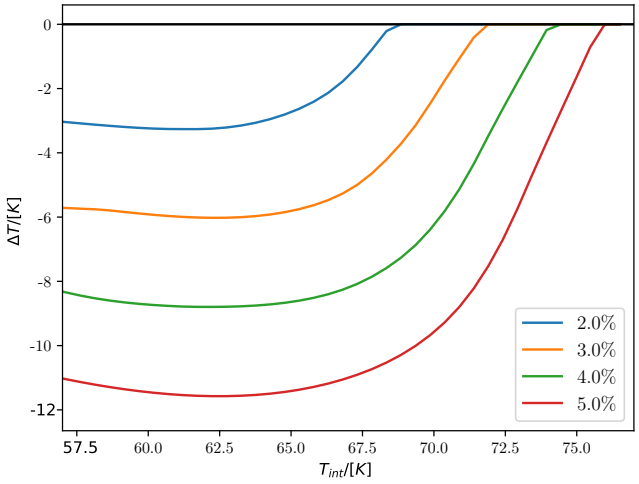

Figure 3: $\Delta T(T_{\rm int})$ for different envelope abundances of methane $q_{\rm max}$ between 2-5%, where $\Delta T \equiv T_e - T_{\rm int}$.

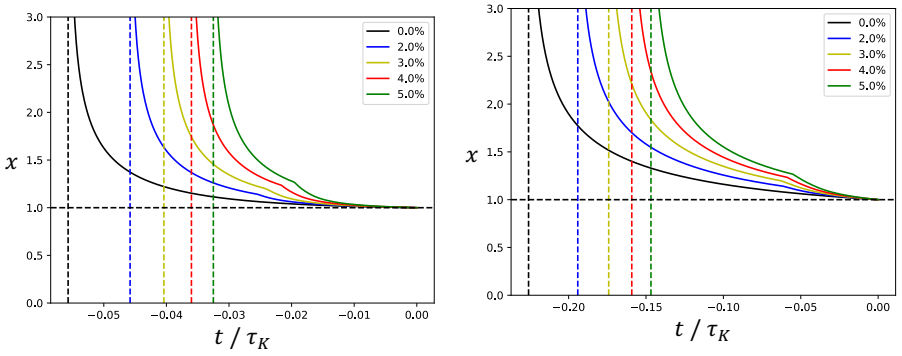

(a) Uranus thermal evolution

(b) Neptune thermal evolution

Figure 4: Thermal evolution model for Uranus and Neptune, with different colored curves representing different methane abundances. The x-axis is the time before the present day, scaled to the relevant Kelvin timescale. The y-axis is x from Equation 13.

mechanism described in Section 2. We can solve for the equilibrium configuration to derive the apparent effective temperature T_e as a function of $q_{\max}$ and T_{int}. These results are shown for methane in Figure 3.

In this section we explore the effect of methane abundances varying between 2-5%. The most commonly cited number for the deep mixing ratio of methane in Uranus and Neptune are 2.3% and 2% respectively, because these are the nominal values in the first published work on the atmospheric structure of these planets derived from radio refractivity data from Voyager [Lindal et al., 1987] [Lindal, 1992]. However, these very works provide solutions to the refractivity data using assumptions of methane abundance between 1% and 4%, finding all these solutions to be theoretically compatible with the observations. Subsequent analysis from ground based and Hubble observations have likewise found a range of acceptable values for both planets ranging between roughly 2%-4% for both planets, finding a range of acceptable solutions as well as latitudinal variation in methane mixing ratio [Baines et al., 1995][Rages et al., 1991] [Baines and Hayden Smith, 1990][Karkoschka and Tomasko, 2011]. In this work we are interested in understanding how thermal evolution is affected by methane condensation. Since the exact mixing ratio is not precisely constrained and we are interested in this question broadly, we take sample value for methane concentration between 2-5% to understand how the effect changes with methane abundance. Unsurprisingly, the effect becomes monotonically more important as concentration increases within this range, as shown in Figure 3 and 4.

Looking at Figure 3 from right to left, we note the following behavior. As the planet cools, the difference between T_{int} and T_e initially grows. This growth occurs because the stable region first expands then moves to deeper, more opaque parts of the atmosphere as it cools. This means a greater temperature difference across the stable region is necessary to accommodate the internal heat flow. This has the effect of rapidly cooling the apparent effective temperature, while slowing the rate of change of the internal equivalent effective temperature. As the planet cools further, eventually ΔT begins to decrease. This is described in more detail in Section 5.

This behavior leads to the evolutionary behavior observed in Figure 4. Before condensation occurs, the planet cools normally. Upon the onset cloud formation, the apparent effective temperature drops rapidly. However, upon reaching the minimum, the apparent effective temperature actually begins to decrease more slowly than the fully adiabatic case. This effect is present in Figure 3 but is more apparent in Figure 5.

5 Effects of water condensation

Water condensation may also inhibit convection using the same mechanism as methane. There are however two important differences: the totally uncon-

strained water abundance in the envelope and the possibility that this water abundance might change substantially over geologic time because of phase transition [Bailey and Stevenson, 2020]. (Of course the second effect might also affect methane–which can partition as water partition because of the Gibbs phase rule–but we ignore this effect for both water and methane). While methane has been unambiguously detected in large abundances in the atmosphere, the presence of water is expected but not proven. The ice giants' gravity harmonics do not require the presence of water–one can construct self consistent interior models using only a mix of hydrogen, helium, and silicates [Helled et al., 2020]. Nevertheless, cosmochemical and formation considerations favor the probable presence of water in the planets' interior. There is no plausible way of accreting a lot of carbon in any form (including CO that would also make water) without also accreting water ice. It is even less certain if water is present in the envelope, and in what abundances. We know from Voyager gravity data that the planet is centrally dense with a less dense envelope, therefore there can't be too much water immediately below the cloud level [Bailey and Stevenson, 2020]. If there is water in the envelope, the expected condensation level is of order 100 bars, therefore condensation occurs in a completely different optical and thermodynamic environment. In this section we consider molar water abundances between 3% and 7% to assess its potential effect on thermal evolution. Somewhat counterintuitively, we find the nominal effect to be in the opposite direction to methane. That is, methane condensation allows the effective temperature of the planet to reach contemporary values from an initially hot state faster, while water condensation causes the planet to take longer to cool to its contemporary state. To understand why, we must inspect the behavior at different internal temperatures.

Figure 5 shows the different between $T_{\rm int}$ and T_e as a function of $T_{\rm int}$. The easiest way to understand what is happening is to consider the limiting case where the stable layer approaches a stable interface. In this case, the temperature difference between the atmosphere above (T_1) and below (T_2) the stable interface is set by the Clausius-Clapeyron relationship, and the critical mixing ratio and bulk mixing ratio $q_{\rm crit}$ and $q_{\rm max}$. In this case we can straightforwardly write down

$$\frac{1}{T_2} - \frac{1}{T_1} = \frac{R}{L} \log\left(\frac{q_{\rm crit}}{q_{\rm max}}\right) \tag{14}$$

Figure 5 shows the exact solution, accounting explicitly for radiative transfer equilibrium, is shown with solid curves while the interface approximation is shown with dashed curves.

To understand why the effect of water is in the opposite direction of methane in the context of cooldown time for Uranus and Neptune, we must look at the shape of the solid ΔT curves in Figures 5. As the planet cools from right to left on these plots, there is initially a decoupling event wherein T_e departs rapidly from $T_{\rm int}$, accelerating the cooling of the planet. However, this occurs when $T_{\rm int}$ is already quite large and cooling is already very rapid, so this acceleration is not very important. As the planet continues to cool, the $\Delta T(T_{\rm int})$ curves begin to

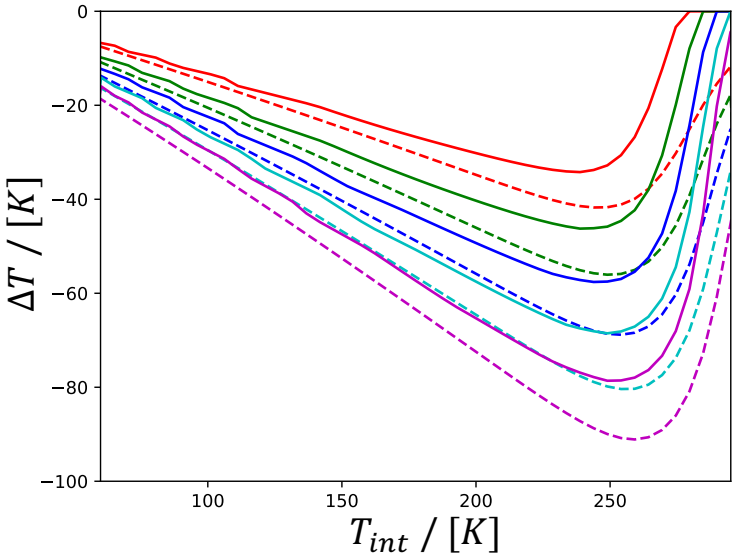

Figure 5: Shows for water condensation the exact solution (solid curves) and interface approximation (dashed curves, Equation 14) for the difference between the apparent effective temperature T_e and the internal equivalent effective temperature $T_{\rm int}$. Colors correspond to different values for $q_{\rm max}$, ascending downward by increments of 1% between 3% and 7%.

have a negative slope. There are two related reasons for this: $q_{\rm crit}$ is temperature dependent, so the right hand side log ratio in Equation 14 becomes smaller as the clouds form at higher temperatures and pressures. Likewise, because the relevant quantity is entropy which scales as $\delta T/T$, this tends to further reduce the effect as T increases. To be explicit, if $T_1 \sim T_2$, we can rewrite Equation 14 as

$$\frac{\delta T}{T} \sim \frac{RT}{L} \ln\left(\frac{q_{\rm max}}{q_{\rm crit}}\right) \tag{15}$$

where $\delta T \equiv T_2 - T_1$. Neglecting moist adiabaticity, we can write $\Delta T/T_{\rm int} \sim \delta T/T$. Using these relationships, we obtain $T_{\rm int} = T q_{\rm max}^{R/c_p} \exp\left[-\frac{L}{c_p}\left(\frac{1}{T_b} - \frac{1}{T}\right)\right]$. In the aysmptotic limit for deep clouds, we find in general $\frac{dT_{\rm int}}{dT} < 1$. Now using $\Delta T/T_{\rm int} \sim \delta T/T$ we find $\frac{d(\Delta T)}{dT_{\rm int}} < 0$ in the asymptotic case, consistent with our results.

This negative slope has important practical applications to evolution. Referring to Equation 11, we see the negative slope of ΔT will translate to a slope of less than unity in $\frac{dx}{dx_{\rm int}}$. This is the reason that for the majority of the planets' evolution, the change in the apparent effective temperature will actually be slowed compared to the case without condensation. The reason water behaves this way but methane does not, is because in the case of the ice giants' contemporary atmospheric temperatures, the methane clouds are either still in the decoupling/accelerated cooling phase where the slope of $\frac{dx}{dx_{\rm int}} \geq 1$. If the planets were to cool still further, for example an ancient rogue planet with $T_e \sim 30$K, then methane would have the same long term effect as water on thermal evolution. Likewise, the intuition for these effects can be straightforwardly mapped onto similar planets in different temperature regimes. For example, an exoplanet planet with a hydrogen atmosphere enriched with water with $T_e \sim 300$K would have its evolution affected in much the same way methane condensation influences the ice giants' thermal evolution. So called 'super-Earths' and 'hot Neptunes' could likewise see a similar effect by silicates. In particular, super-Earths with hydrogen envelopes, if cooling from an initially saturated or well-mixed state, could exhibit an extreme version of this behavior as $q_{\rm max} \to 1$.

5.1 Simultaneous consideration of two cloud levels

If both methane and water cloud levels inhibit convection, then both effects must be accounted for simultaneously in the model. In order to solve this, we solve for the radiative heat flow at both the methane and water condensation levels to be in equilibrium with the final effective temperature. We assume the sunlight is absorbed below the methane condensation level, but above the water condensation level. The solution to $T_e(T_{\rm int}, q_m, q_w)$ is shown in Figure 6. This figure shows one of the major points of this work: knowing the external temperature does not necessarily tell you the internal temperature. Taking as an

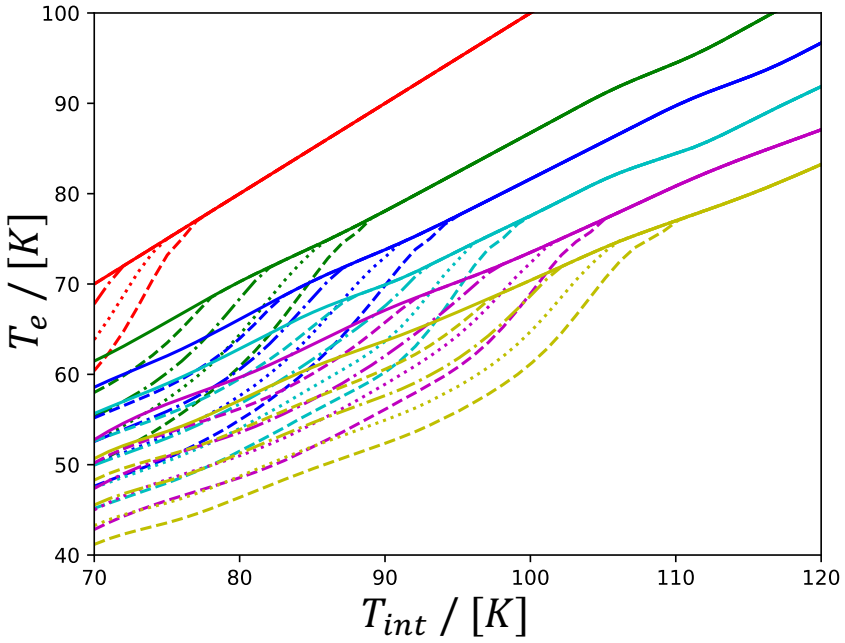

Figure 6: Apparent effective temperature T_e as a function of internal equivalent effective temperature $T_{\rm int}$ considering both methane and water. Colors correspond to water abundance, increasing downward from 0% to 7% water. The curve style corresponds to methane abundance, increasing downward from 0% to 5% abundance. This figure illustrates the immense uncertainty in the internal equivalent adiabat even with a precise effective temperature measurement.

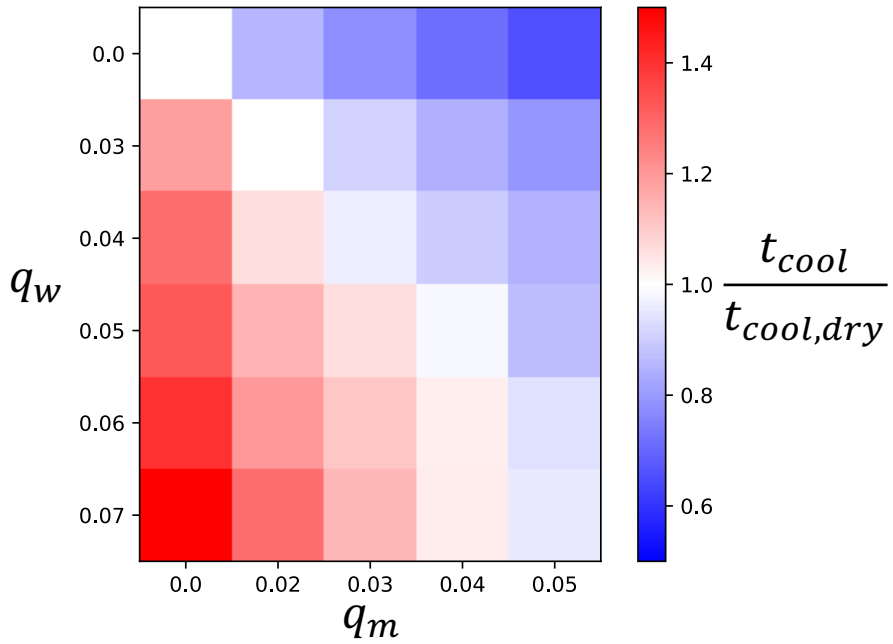

Figure 7: Shows the ratio of the cooldown time from an initially hot state to its current state compared to the case that neglects convective inhibition for a cross section of water abundances q_w and methane abundances q_m. Of course this is unity when $q_w = q_m = 0$.

example $T_e = 60$K, we see $T_{\rm int}$ can plausibly be anywhere between $60 - 100$K, a huge range in terms of the assumed thermodynamic state of the interior. This has important applications for both interior modeling, where modelers should seriously consider the possibility that the interior is significantly hotter than the exterior would lead one to expect, as well as for thermal evolution considerations, the primary focus of this paper.

The effect on thermal evolution is a surprisingly straightforward superposition of what we found for each condensate species separately: the more methane you add, the faster a planet can cool from an initially hot state to its current state. The more water you add, the longer it takes for the planet to cool to its current state. The two effects can be in opposite directions such that the overall effect is nearly canceled. The behavior is shown in Figure 7.

6 Discussion

Convective inhibition by condensation in hydrogen atmospheres plays a profoundly important role in thermal evolution. Depending on the abundance,

methane condensation may accelerate the cooldown time from an initially hot state to contemporary states by nearly a factor of two by decoupling the atmosphere from the interior. On the other hand, water condensation slows thermal evolution by preventing heat from efficiently escaping. Interior composition modelers should bear in mind that the internal 1-bar equivalent temperature may depart from simple adiabatic extrapolation of the troposphere by nearly a factor of two (see Figure 6).

As mentioned in Section 5.1, as the planets continue to cool methane will begin to behave similarly to water, exhibiting the characteristic turnover in $\Delta T(T_{\rm int})$. As this occurs, it will prevent heat from escaping and slow further thermal evolution. One implication of this behavior is that we expect the planets to be in a somewhat special state with the methane clouds near the 1 bar level. This state actually persists for much longer from a thermal evolution perspective than an arbitrary/random thermal state. When the planet cools to a temperature somewhat warmer than this state, the atmosphere will decouple. After the atmosphere decouples, the slope inverts, slowing further cooling. Therefore these planets will spend a longer portion of their thermal lives in the state where the methane cloud level is $\sim 1-10$bars than they would in a thermal evolution model that does not consider convective inhibition by methane condensation. Perhaps this consideration renders the surprising similarity of Uranus and Neptunes' atmospheres' shallow temperature structures despite their vast difference in insolation somewhat less improbable than it might first appear.

It is important to consider whether this atmospheric structure is compatible with existing data, especially Voyager radio refractivity data. The current data has been shown to be consistent with many different models, including subadiabatic, adiabatic, moist adiabatic, and superadiabatic temperature gradients [Helled et al., 2020]. The data has also been shown to be compatible with a wide range of temperature structures and methane abundances [Lindal et al., 1987][Lindal, 1992]. The data itself shows a layer of rapidly varying refractivity near the condensation level, generally interpreted to be methane clouds [Lindal et al., 1987][Lindal, 1992][Marley and McKay, 1999]. Another interpretation of the same data supports a layer of superadiabatic temperature lapse rate in the cloud-forming regions of these planets [Guillot, 1995]. In general, our understanding of the thermal structure of the ice giant atmospheres is incomplete, as the results from Voyager 2 refractivity data are model dependent, with a particular degeneracy between assumed methane enrichment and temperature structure. In order to disentangle these variables and have a more confident understanding of these planets' atmospheres' thermal structures, we must return with a mission. It should be a priority for a future mission to independently measure methane abundance and temperature, perhaps with entry probes or a well designed microwave radiometer experiment.

These general findings do not consider the long term stability of stable layers in the atmosphere. As long as the stability timescale is greater than the

relaxation timescale for a stable layer, the results should approximately reflect reality. If that condition is satisfied, then even if stable layers are intermittently interrupted by massive internal plumes, large meteor impacts, or instability due to long term erosion by entrainment, they will reform again on geologically short timescales ($\sim$ 100yr). Therefore the thermal evolution will be governed primarily by the equilibrium state, and not possible intermittent periods of enhanced activity. Intermediate states where the equlibrium configuration is thinned over time but not totally destroyed by entrainment erosion would in general reduce the magnitude of $\Delta T(T_{\rm int})$, so the findings in this paper should be considered an upper bound.

If there are indeed layers of static stability in the troposphere or deep atmosphere of Uranus and/or Neptune, then they should support gravity waves. Whether we expect gravity waves to be excited, what their general characteristic would be, and whether they could be detected from space (for example using an Doppler imager) is a subject worthy of future theoretical consideration.

Whatever the uncertainties about the specifics, the basic physical mechanism is probably important in the ice giants because of their highly enriched atmospheres. There may be additional stable layers, for example a silicate cloud level beneath the water cloud level, or a sulfide/ammonia cloud level. We focus on only two in this work to demonstrate the general principle without getting bogged down in largely unconstrained assumptions about the envelope enrichment in each species. However, the intuition we build here for methane and water can be straightforwardly applied to other cloud levels using exactly the same method. This method is also likely to be applicable to the majority of exoplanets, ranging from super-Earths with hydrogen envelopes to metal-enriched gas giants. It is clear from this work that thermal evolution and internal thermal structure may be profoundly influenced by convective inhibition by condensation. Any complete model of thermal evolution or internal structure must consider convective inhibition.

References

Bailey, E. and Stevenson, D. (2020).

Baines, K. and Hayden Smith, W. (1990). *Icarus*, 85:65–108.

Baines, K., Mickelson, M., Larson, L., and Ferguson, D. (1995). *Icarus*, 114:328–340.

Fazio, G., Traub, W., Wright, E., Low, F., and Trafton, L. (1976). *ApJ*, 209:633–657.

Fortney, J., Ikoma, M., Nettelmann, N., Guillot, T., and Marley, M. (2011). *ApJ*, 729(32).

Friedson, A. and Gonzales, E. (2017). *Icarus*, 297:160–178.

Guillot, T. (1995). *Science*, 269:1697–1699.

Guillot, T. (2005). *AREPS*, 33:493–530.

Gulkis, S., Olsen, E., Klein, M., and Thompson, T. (1983). *Science*, 221(4609):453–455.

Helled, R., Nettelmann, N., and Guillot, T. (2020). *SSRv*, 216(38).

Hubbard, W. (1977). *Icarus*, 30(2):305–310.

Hubbard, W. (1978). *Icarus*, 35:177–181.

Hubbard, W., Guillot, T., Marley, M., Burrows, A., Lunine, J., and Saumon, D. (1999). *P&SS*, 47:1175–1182.

Hubbard, W. and MacFarlane, J. (1980). *JGR*, 85(B1).

Karkoschka, E. and Tomasko, M. (2011). *Icarus*, 211:780–797.

Kellermann, K. and Pauliny-Toth, I. (1966). Observations of the radio emission of uranus, neptune, and other planets at 1.9cm. *ApJ*, 145(3):954–956.

Leconte, J., Selsis, F., Hersant, F., and Guillot, T. (2017). *A&A*, 598.

Li, C. and Ingersoll, A. (2015). *NatGe*, 8:398–403.

Lindal, G. (1992). *ApJ*, 103(3).

Lindal, G., Lyon, J., Sweetnam, D., Eshleman, V., et al. (1987). *JGRA*, 92(A13):14987–15001.

Linder, E., Mordasimi, C., Molliere, P., Dominik-Marleau, G., Malik, M., et al. (2019). *A&A*, 623(A85).

Loewenstein, R., Harper, D., and Moseley, H. (1977). *ApJ*, 218:L145–L146.

Marley, M. and McKay, C. (1999). *Icarus*, 138(2):268–286.

Nettelmann, N., Wang, K., Fortney, J., Hamel, S., Yellamilli, S., et al. (2016). *Icarus*, 275:107–116.

Pearl, J. and Conrath, B. (1991). *JGR*, 96:18921–18930.

Pearl, J., Conrath, B., Hanel, R., Pirraglia, J., and Coustenis, A. (1990). *Icarus*, 84:12–28.

Podolak, M., Hubbard, W., and Stevenson, D. (1991). Models of uranus' interior and magnetic field. In *Uranus*, pages 29–61. University of Arizona Press, Tucson, AZ.

Rages, K., Pollack, J., Tomasko, M., and Doose, L. (1991). *Icarus*, 89:359–376.

Scheibe, L., Nettelmann, N., and Redmer, R. (2019). *A&A*, 632(A70).

Stevenson, D. (1983). *JGR*, 88(B3):2445–2455.

Stier, M., Traub, W., Fazio, G., Wright, E., and Low, F. (1978). *ApJ*, 226:347–349.